CASL-U-2013-0214-000

Power uprates
and plant life extension

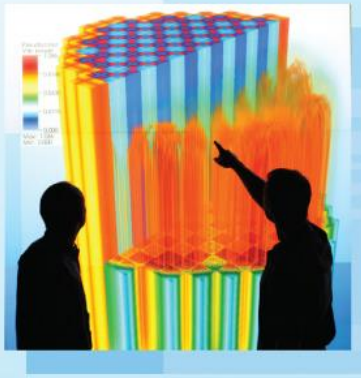

Engineering design
and analysis

Science-enabling
high performance
computing

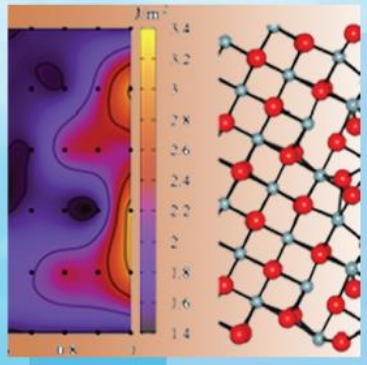

Fundamental science

Plant operational data

Consortium for Advanced Simulation of LWRs

# L3:THM.CLS.P7.08
# Experimental Investigation of Subcooled Flow Boiling

Yassin A. Hassan
TAMU

September 30, 2013

U.S. DEPARTMENT OF ENERGY | Nuclear Energy

TEXAS A&M UNIVERSITY

# Experimental Investigation of Subcooled Flow Boiling

## Milestone Report

**PI: Yassin A. Hassan**

**9/30/2013**

CASL-U-2013-0214-000

# Contents

Introduction ..... 5

Experimental Setup ..... 7

Hydraulic Loop ..... 7

Visualization System ..... 9

Temporal Multi-Scale Approach ..... 9

Spatial multi-scale approach ..... 11

Experiments ..... 12

PTV-IR-Shadowgraphy experiments ..... 12

Results ..... 13

Bubble intermitency ..... 16

Effect of laser illumination and timing modes (Straddling vs Continuous) ..... 17

Velocity Measurements ..... 18

Liquid Velocity Statistics ..... 19

Conclusions ..... 22

Subcooled Flow Boiling Through a Square Channel

***Principal Investigator: Yassin A. Hassan***
***Texas A&M University***
***Nuclear Engineering Department***
***Phone: (979)845-7090; E-mail: Hassan@ne.tamu.edu***

---

## *Objective*

The Consortium for Advanced Simulation of Light Water Reactors (CASL) and Texas A&M University joined research efforts to perform high performance simulations of subcooled boiling flow within PWR assemblies. Texas A&M University is in charge of obtaining experimental data to support the validation of CFD codes mechanistic models for two-phase flow simulations. Several experimental benchmarks were designed to achieve this goal. The experimental development, results and project status are presented in this document.

## *Approach*

Use state of the art non-intrusive visualization techniques to obtain high accuracy and fidelity measurements. The experimental techniques used in this work are: Particle Image Velocimetry (PIV), High Speed Shadowgraphy (HSS), and Infrared Thermometry (IT).

## *Accomplishments*

Performed a series of sensitivity studies to identify practical issues that may hinder the measurement accuracy. Based on these studies, an experimental protocol was established to reduce errors and ensure measurements repeatability.

The measured quantities can be divided depending on the measured phase. For the liquid phase, the following quantities were measured: Liquid turbulence statistics such as: 2D velocity and vorticity fields, turbulence intensities and Reynolds stresses. For the gas phase, bubble dynamics parameters such as: departure diameter, growth rate, and velocity are readily available.

The measured two-phase flow parameters are being used to develop empirical and semi-empirical correlations that will help predict the liquid behavior close to the heater wall.

## *Future Direction*

Currently performing analysis of experimental shadowgraphy data to account for more experimental conditions. These experiments were performed without the PIV laser light, and were designed to provide reliable measurements of the dynamics of the boiling bubbles. Therefore no additional quantification of the laser heat needed to be considered. Also the IR thermometry measurements are currently being analyzed by including a “correction” to account for the multilayer radiation problem.

---

## Introduction

Turbulent subcooled boiling flow has been used extensively in industry because it is one of the most efficient heat transfer modes. The continuous mixing and stirring of liquid produced during the life cycle of the subcooled boiling bubbles due to nucleation, growth, detachment, coalescence and collapsing are enhancing mechanisms of heat and momentum transfer. Necessarily, the understanding of two-phase flow parameters and their impact on the liquid turbulence plays a key role in the prediction of complex flow behaviors, safety analysis and design of the high energy systems found in industry. In particular, the nuclear industry relies on the accurate prediction of local two-phase flow parameters. For example, the nucleation sites location and the amount of void within coolant/moderator sub-channels affect not only the reactor's reactivity, but also promote the crud formation which has been shown to contribute to the generation of heat transfer non-uniformities along the fuel rods and ultimately fuel rod structural failures. Although multiple experimental efforts has been directed towards the understanding of subcooled boiling flow, the complexity of the phenomenon and its high dependence on the experimental conditions has produced large discrepancies among experimental results, even at similar conditions.

Therefore there is a need of innovative experimental techniques that can fulfill the demanding statistical requirements to describe the stochastic nature of subcooled flow boiling. This work explores the scope and limitations of innovative measuring techniques to study subcooled boiling flow. Efforts for the simultaneous measurements of liquid and vapor parameters and their interactions are described. Emphasis is given to achieve measurements with the required temporal and spatial resolutions for both: average and fluctuating quantities.

Multiple efforts have been attempted to measure local fields of subcooled boiling parameters of the liquid phase (Roy et al. 1993; Lee et al 2002; Situ et al 2004). Based on the experimental information from the

previous studies, different two-phase flow models were developed (Koncar & Tiselj 2008; Koncar & Krepper 2008; Koncar & Matkovic 2012; Končar et al. 2004; Ramstorfer et al. 2008; Roy et al. 2002) with some success. These models share the characteristics of being based on time-average analysis of information from point measurements probes. However, due to the complex nature of the turbulence found in subcooled boiling, this approach seems to be limited. A full-field measurement approach is needed to provide the required spatial and temporal information. Visualization techniques such as Particle Image Velocimetry (PIV) and Particle Tacking Velocimetry (PTV) can be used to overcome some of the limitations associated with point measurements techniques. Estrada-Perez and Hassan (2010) performed PTV experiments in a square vertical channel with a single heated wall. Their results confirmed the behavior found in previous studies and provided new information due to the full-field nature of the technique. The new provided information has already been used towards the development of a two-phase wall law and for CFD simulation validation Koncar and Matkovic (2012). The present study is a continuation of the experimental endeavor started by Estrada-Perez and Hassan (2010), and has the objective of extending the measurements capabilities to overcome some of the measurement limitations by conducting simultaneous PIV, Shadowgraphy and Infrared thermometry to fully account for local and global changes present in subcooled flow boiling. This work is an attempt to provide high-quality data of turbulent subcooled boiling flow for validation and improvement of two phase flow computational models.

## Experimental Setup

The experimental facility was designed for the visualization of subcooled boiling flow of refrigerant HFE-301 at low system pressure. The facility consists of a hydraulic loop and a visualization system. Experimental setup details are given in the following sections.

### Hydraulic Loop

The hydraulic loop consists of an external loop and a test section, both designed to withstand temperatures in excess of 200 $^{o}$C, and pressures up to 100 psi. The external loop provides thermal and hydraulic steady state conditions. The system excess energy is removed with a small plate heat exchanger connected to a chilling system. This allows us to have control of the inlet temperature to the test section. The mass flow rate to the test section was measured with a Coriolis flow meter and controlled by adjusting the test section valves. The test section is a rectangular channel made of transparent polycarbonate, with 30.5 mm length and a cross-sectional area of $10 \times 10$ mm$^{2}$. Energy for boiling is provided through a transparent ITO heater with a length and width of 25.5 cm and 9 mm, respectively, and a maximum working temperature of about 200 $^{o}$C. The heater is attached to the lateral interior face of the channel (see Figure 1). The electric current to the heater is provided and adjusted by a DC power supply. To reduce heat losses to the ambient, an insulation system made of transparent polycarbonate and a saphire windows covered the test section.

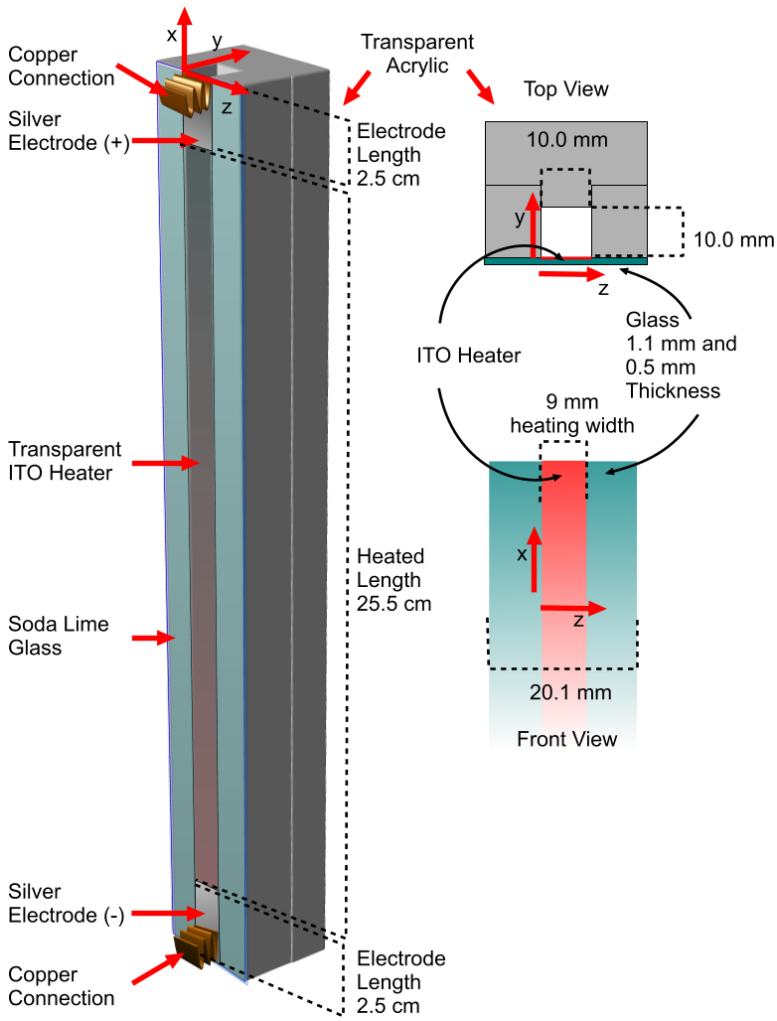


**Figure 1. Test section schematics and dimension**

The insulation system material was chosen to provide visual access for both the IR-cameras and the High speed camereas. An unheated length of about 61 cm was considered before the test section (i.e., L/D~61) to ensure fully developed flow. To measure the heater wall temperature, a midwave infrared high-speed camera (3-5 μm) was used. A K-type thermocouples was attached to the external face of the heater, to provide validation for the Infrared camera measurements. The test section fluid inlet ($T_{in}$) and outlet ($T_{out}$) temperatures were measured with two fast response T-Type thermocouples. Figure 1 shows the schematics and dimensions of the test section.

## Visualization System

The visualization system consisted of a high-speed high-resolution camera, a high-speed high-power laser, a high-speed infrared camera, a fast response LED illumination system, mirrors, translational stages, lenses, optical filters and particle flow tracers. The flow tracers are fluorescent particles with density range of 1.39 to 1.41 g/cm, with an average particle diameter of 5 $\mu$m. The high-speed camera has a maximum frame rate of 6000 fps at a resolution of 1024x1024 pixels, with a maximum bit depth of 12 bits. The illumination was provided by a Pegasus dual lamp laser which can operate at a maximum power of 27 mJ/pulse. A maximum pulse rate of 20,000 pulse/s can be achieved. Two optical mirrors and two concave-convex lenses are used to convert the small circular beam from the laser, into a thin sheet of light. The laser light sheet is positioned on the measurement region, parallel to the camera focal area. The LED system is externally synchronized to be used as the shadowgraphy illumination. The camera, mirrors and lenses are mounted on translational stages to have the capability of changing the measuring region along the test section. Figure 2 shows the schematics of the visualization system. The High speed cameras, the laser and the LED illumination system are synchronized in such a way as to be able to obtain quasi-simultaneous PIV and Shadowgraphy measurements.

## Temporal Multi-Scale Approach

The configuration shown in Figure 2 was designed as to allow multi-orientation and multi-scale measurements. The high speed PIV-Shadowgraphy camera is arranged to provide “semi-simultaneous” measurements of PIV and shadowgraphy. This is achieved by synchronizing the camera shutter with alternating pulses of laser and led illimination.

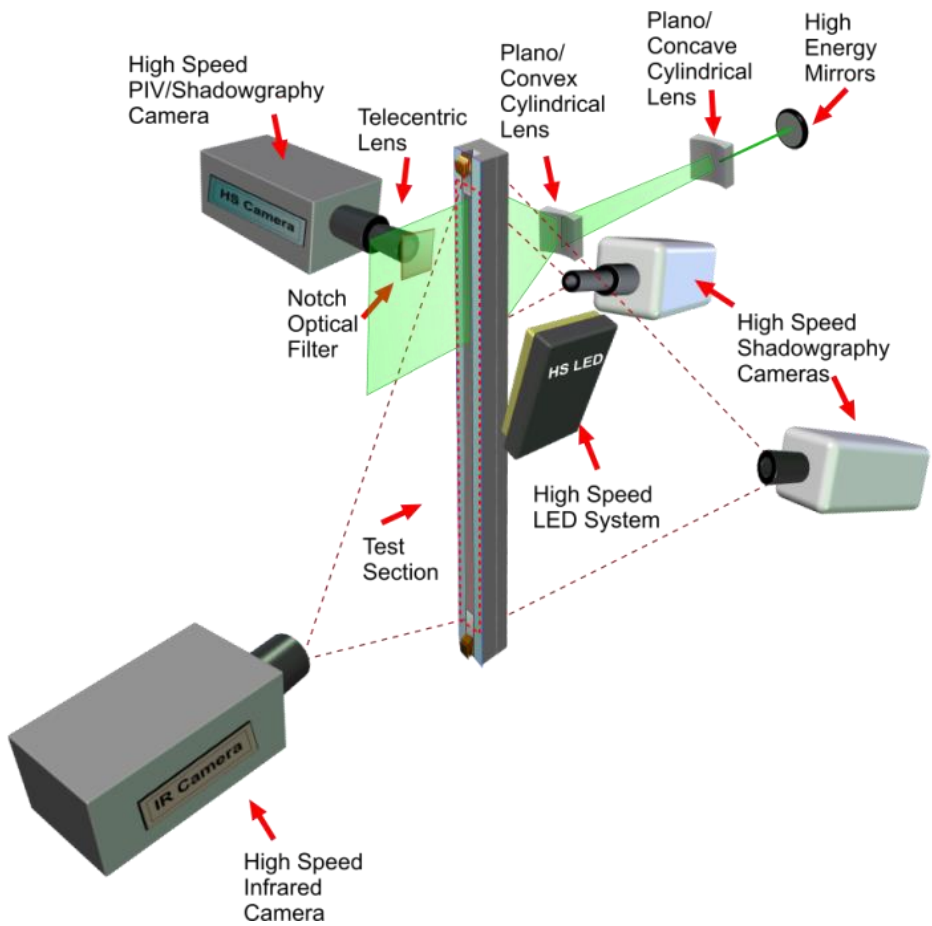


**Figure 2 Visualization system schematics**

From the temporal multi-scale point of view, the PIV/Shadowgraphy camera can be configured to run in continous or in straddling modes.

Continuos mode provides a fixed time interval between each consecutive frame. In order to properly capture the fast moving features within the flow, this time interval ($\Delta t_{PIV}$) need to be small and consequently the camera need to be run at high speeds. Due to the camera memory limitations the continuos configuration provides short measuring times of the order of fractions of a second. This limited measuring time also limits the capability of measuring  accurately time-average flow quantities.

Straddling mode combines a small time interval (small $\Delta t_{PIV}$) between image pairs plus a waiting period which will be called straddling time ($\Delta t_{Straddling}$). This waiting period is required to achieve a higher number of independent samples while increasing the measuring interval. Similarily, the two high speed shadowgraphy images can also be configured to work in either continuos or straddling modes. Figure 3 shows an eschematics of the timing used to achieve "semi-simultaneous" PIV and Shadowgraphy images. The green squares represent camera frames illuminated with the PIV laser, while the gray squares represent the camera frames illuminated only with the LED lamp. The white squares represent the "waiting" period or stralling time ($\Delta t_{Straddling}$). As shown in Figure 3, the "semi-simultaneous" PIV/Shadowgraphy experiment consists of sets of four frames each. Two frames for PIV and two frames for shadowgraphy. The time interval between a PIV and a Shadowgraphy frame is given by $\Delta t_{Straddling}/2$.

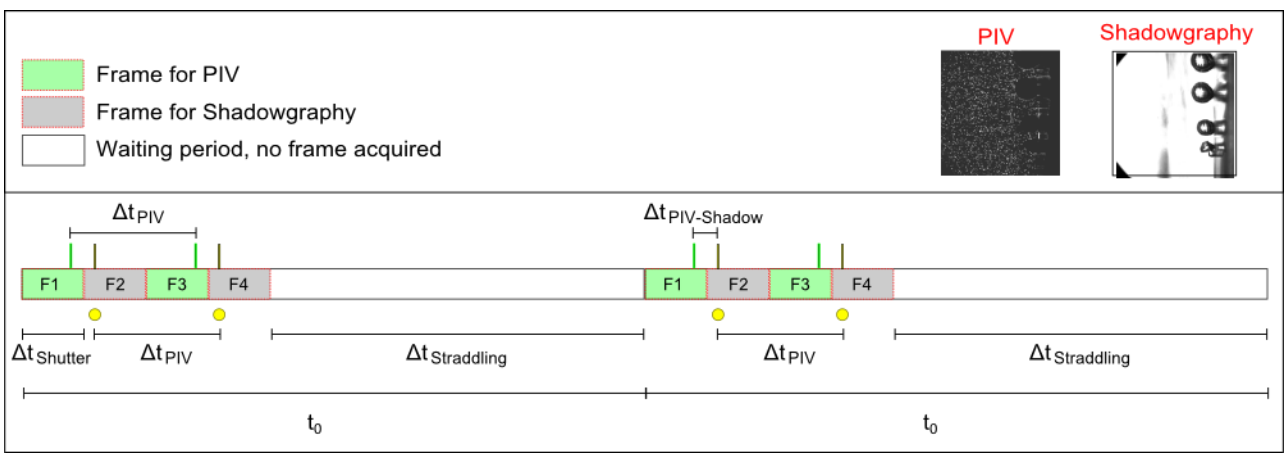


**Figure 3 Timing configuration for "semi-simultaneous" PIV/Shadowgraphy measurements**

## Spatial multi-scale approach

To achieve spatial multi-scale measurements, a telecentric lens was used which allowed the selection of two different visualization modes: High and medium magnification modes, which correspond to a resolution of 4.82 and 17.5µm respectively. The shadowgraphy cameras are configured to have different visualization modes: one set as high magnification while the other at low magnification. The low

magnification corresponds to a resolution of 187μm. In this report, we will focus on the results from the medium-magnification PIV/Shadowgraphy which is the only one that provides simultaneous information from both phases (liquid and vapour).

## Experiments

### PTV-IR-Shadowgraphy experiments

The measurement area was located at about 12.3 cm from the test section inlet. Simultaneous PTV and shadowgraphy measurements were performed at this position. The high-speed camera was set to a $\Delta t_{PIV-Shadow}$ = 1/4000, or 4000 frames/s, with an exposure time of 250μs. The relatively large exposure rate was selected as to allow enough light to reach the camera sensor and achieve satisfactory shadowgraphs of the bubbles. The time between each PIV pair and each shadowgraphy pair was $\Delta t_{PIV}$=1/2000. This timing allows to take one frame of PIV imediatelly followed by one frame of shadowgraphy. Each acquired image consisted of 640×952 pixels. As of today, only one Reynolds number has been considered, Re = 4400. For this Reynolds number, a heat flux of $q''$=13.5 kW/m$^2$ was selected and a constant inlet temperature of 10 $^{o}$C was maintained. This experimental condition allowed for a stable nucleation site behaviour, however, as can be seen later, a nucleation intermitency was noticed when repeating the experiment. The heater wall temperature was measured with the infrared camera. The infrared camera magnification allowed temperature measurements of the wholelength of the test section. Inlet and outlet fluid temperatures were also measured by means of T-type hypodermic thermocuples.

## Results

Figure 4 and Figure 5 show typical experimental images obtained with shadowgraphy and PIV techniques respectively. As can be seen in the raw (cropped) Shadowgraphy image in Figure 4(a) the bubbles are depicted as dark moving object embedded in a lighter background. Although an ideal bubble shadowgraph should be a black spheroid in a white background, the bubbles images from the current experiment shows a transparent center which makes the image pre-processing more difficult. The difficulty arises when trying to discriminate the background from the bubbles, the transparent center of the bubble will present similar characteristics as that of the background, making it difficult the discrimination between them. This deviation from ideal shadowgraphs was due to the fact that the led illumination was not perfectly parallel to the camera sensor.

The shadowgraphy images presented specific difficulties, the following issues were found: (a) Uneven background (b) bubbles centers showed to have similar brightness properties compared with the background (c) Liquid density changes affected the refractive index of the liquid making background fluctuations difficult to identify and remove.

To overcome the aforementioned difficulties, the following image processing algorithm was developed and applied to the shadowgraphy images.

a) Original Image.
b) Inverted Image – “a” image (with 2 iterations) ---> b=[a^(-1)-a]
c) "b" images - Average from 1000 "b" images ---> c = [b - b_{avg}_{1000}]
d) "c" images with preferential and thresholded horizontal shadow ---> d=shadow(c)
e) fill holes (using imageJ) of "d" images ---> e=fillholes(d)
f) Find centroid using gray scale thresholding ---> f=FindCentroids(e)
g) Track bubbles centroid velocities ---> g=Track(e_1, e_2)

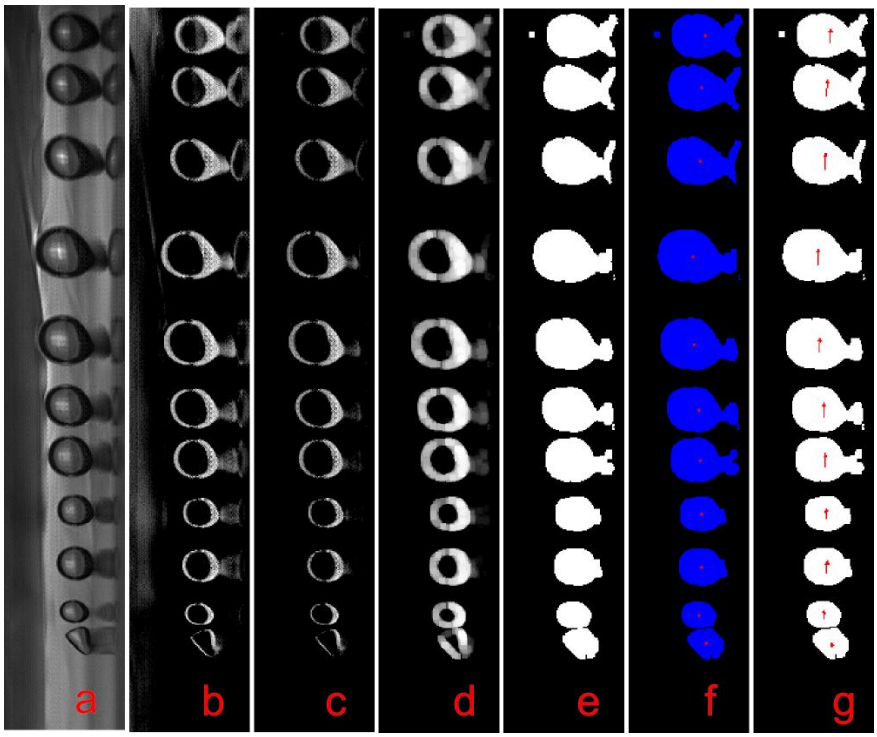


**Figure 4 Shadowgraphy Image pre-processing for bubble dynamics measurements**

Figure 5 shows the PIV images together with the image processing required to extract accuratelly the liquid velocity vectors. The raw PIV image is depicted in Figure 5(a). The PIV images are characterized by the white seedings in a dark background, In this case the laser light was positioned on top of the nucleation site. It is clear from  Figure 5(a) the edge of the bubbles being illuminated by the laser. Ideally, when a bubble is pressent, only the bubbles edges should be visible, however in some instances, the bubble body will contain white spots that the PTV algorithm will detect as moving particles. From the particle detection and particle tracking process point of view, the following issues were found: a) Bubbles reflections. b) Bubbles transparency produced the effect that particles existed within the bubbles. Consequently velocity vectors are found by the PTV algorithm on top of the vapor phase region. c) Liquid density changes affected the refractive index of the liquid, therefore the particle images suffered of distortions. d) Elongated particle images are the result of large density gradients in regions close to the wall.

To overcome the aforementioned difficulties, the following image processing algorithm was developed and applied to the original PIV images.

a) Original Image.
b) “a” Image - Bubbles Information (from step “e” of theshadowgraphy image process)
---> b=[a-e*]
c) particle centroids locations using image pattern matching c = find particles(b)
d) with particles found in two consecutive images, the particle tracking is performed using a direct cross correlation technique.

The final result is a velocity field of the liquid phase without the influence of the bubbles noise. Figure 5(d) shows the effectiveness of the algorithm. There are virtually no velocity vectors on regions occupied by the bubbles.

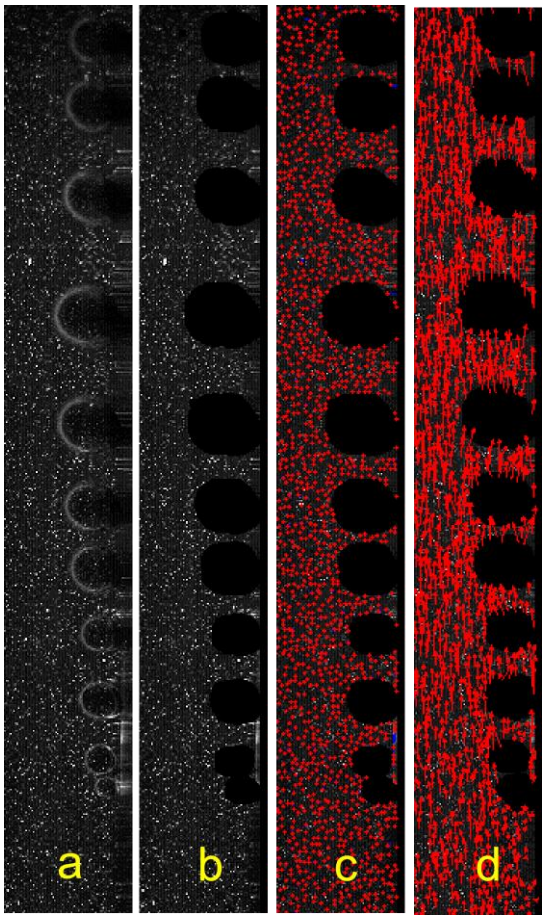


**Figure 5 PIV Image pre-processing for liquid velocity measurements**

It is important to mention that the camera lens is equiped with a notch filter with a band pass within the range 527 +/- 15 nm. The notch filter blocks most of the laser ligth, and therefore helps to reduce the undesired reflections from the bubbles. This in turns allows a more accurate liquid velocity measurement, since the spurius vectors produced by the bubbles reflections are notabely reduced.

## Bubble intermitency

Although it appeared that at this experimental condition a stable bubble nucleation behavior was achieved, the influence of the additional power supplied by the laser showed to be large. When performing PIV experiments in a continuous mode (see timing configuration explanation), the nucleation site behavior changed drastically (these effect will be explained in later sections). Therefore it was decided to perform the PIV experiments only in straddling mode configuration. In straddling mode, the laser induced power was largely reduced, and the effect of the laser in the nucleation behavior was not longer noticeable. However, some intermittency was observed in the activity of the nucleation site. As shown in Figure 6, this intermittency was detected directly from the experimental images. Ten percent of the 10,000 PIV images were considered as “intermittent” instances on which a lower void fraction was found. Examples of what was considered an “intermittent” image are shown in Figure 6 (A), (B), and (C). Intermittent images were removed from the analysis of flow statistics because they were not representative of the “stable” behavior of the nucleation site. Figure 6 (D) and (E) are examples of the experimental data that was considered in the statistical analysis. As of today, is not known with certainty the reasons of this intermittency.

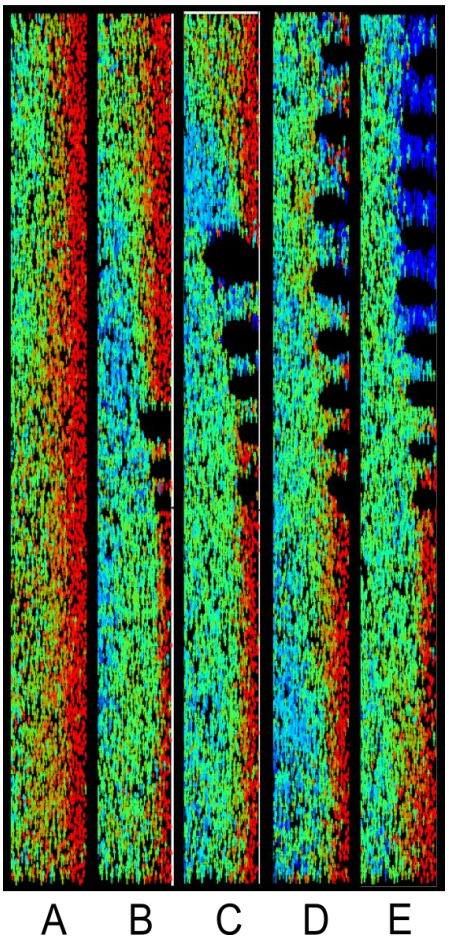


Figure 6 Intermittency of nucleation site activity.

## Effect of laser illumination and timing modes (Straddling vs Continuous)

As mentioned previously, the laser induced power has a large effect on the nucleation site behaviour. Therefore, a sensitivity analysis was performed to quantify this influence and to explore ways to minimize non-desirable effects. Four tests with different timing modes and illumination types wereperformed: a) LED illumination and continuous timing mode, b) LED illumination and straddling timing mode, c) LED+laser illumination and Continuous timing mode, and d) LED+laser illumination and Straddling timing mode. For this analysis, we focused on the bubles dynamics behavior. From this analysis it was concluded that as long as the straddling timing mode is used, non-desirable influences from the illumination are considered to be negligible small.

## Velocity Measurements

After addressing the issues that may have hindered the statistics reliability, we focused on the liquid and bubbles statistics. The velocity of both phases was obtained by means of particle tracking velocimetry (PTV). The PTV algorithm is able to track small objects such as the PIV particle tracers or large objects such as the boiling bubbles.  The results of the tracking algorithm are shown in Figure 7. The picture in the left of Figure 7 shows an instantaneous velocity field on top of the shadowgraphy image, the right picture in Figure 7 shows the PTV results of the boiling bubbles. The picture in the center of Figure 7 shows the average liquid and bubbles axial velocity profiles along the axis of the heater.

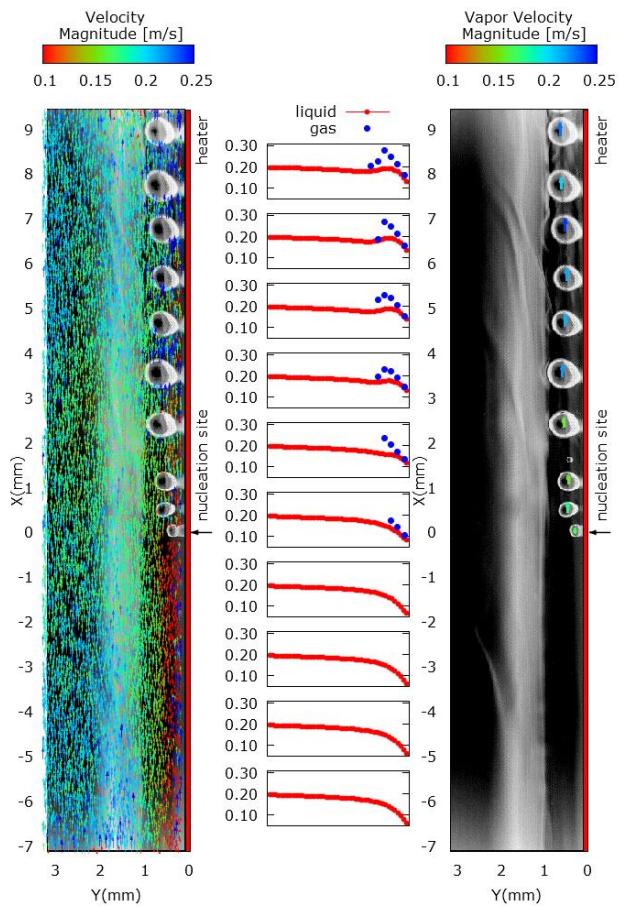


**Figure 7 Liquid and bubbles velocity fields and profiles**

Figure 7 shows the advantages of using the single nucleation site approach. This approach provides the capability of measuring at the same experimental conditioin, the  flow development from a heated single phase to the transition to two-phase boiling flow. Furthermore, the bubbles dynamics can be accurately characterized at every point along the heater, this allows to explore the influence of multiple bubble dynamics conditions on the average liquid velocity behaviour. In specific it Is explored the relationship between bubbles diameters and velocities with the liquid behaviour along the heater. From Figure 7 it is clear that the effect of the nucleated bubbles brought significant changes on the liquid behaviour: Upstream of the nuclation site, in the single-phase region, the liquid velocity is virtually not affected, the liquid statistics remain the same at different axial positions. Such behaviour remain constant up until the regionon which the nucleation site is located. Downstream the nucleation site, there is a liquid axial velocity increase which seems to be concomittant to the bubbles sizes and velocities. From the present observations it appears that the liquid velocity increase with the distance is mainteined up until about a distance of 7 to 8mm, after which, the local peak of liquid velocity tend to a terminal value of 0.2 m/s. A similar behaviour was observed for the boiling sliding bubbles, bubbles diameters and velocities increased concomittantly with the distance. This increase on bubble diameter is attributed to the bubble sliding through the heated wall. It was also observed that the rate of bubble grouth is much larger near the viscinity of the nucleation site, and that after few millimiters (~4 mm), the bubbles dimensions reached a value that was kept relativelly constant. Bubbles velocity depended entirely on the bubbles sizes along the heater.

## Liquid Velocity Statistics

One of the main objectives of the PTV measurements is to obtain detailed information of the liquid velocity close to the heated wall under subcooled boiling conditions. Previous works had attempted to obtain two phase flow logarithmic laws that fully describe the liquid velocity under the influence of the dispersed

phase (Marie et al. 1997; Mikielewicz 2003; Sato & Sekoguchi 1975), based on the roughness theory In other works, attempts to relate the boiling bubbly flow as a type of roughness has been attempted (Krogstadt & Antonia 1999; Osterlund et al. 2000), and some models were proposed for the simulation of subcooled boiling (Koncar & Krepper 2008; Koncar & Tiselj 2010), however there is still a lack of detailed information to accurately quantify the effects of boiling bubbles into the liquid behavior, therefore in this work, using the experimental results of the single nucleation site experiment, an attempt to describe the behavior of the liquid under different void fraction conditions was performed. Figure 8 shows the average axial velocity profile at different locations from the wall. The color bar indicate the axial distance from the nucleation site, starting with the light blue for locations on which only single phase flow is located, the darkest blue represents the location after 8mm downstream the nucleation site. It is clear the influence of the boiling bubbles on the liquid velocity. There is a local peak in the region close to the wall. This local peak is related to the average bubble radius measured at each axial location.

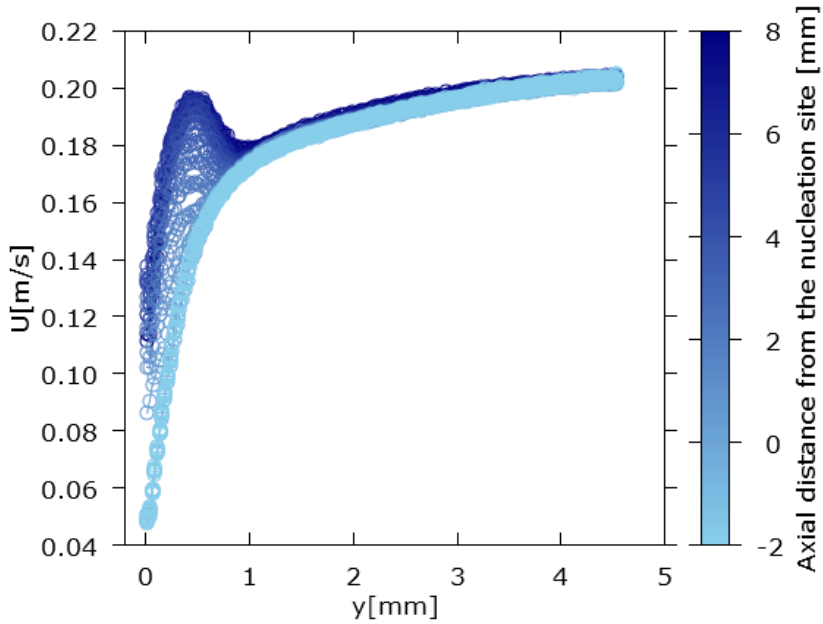


**Figure 8 Axial liquid velocity profile at different axial positions from the nucleation site.**

To have a better understanding of the liquid behavior, it is always convenient to present these results in dimensionless form. The characteristic length and velocity used for the non-dimensionalization are $y^+ = yu_\tau/\upsilon$ for the characteristic length and $u_\tau$ for the characteristic velocity, $u_\tau$ is the friction velocity defined as $u_\tau = \sqrt{\tau_w/\rho}$ . The wall shear stress $(\tau_w)$ is obtained experimentally using the approximation for regions close to the wall as $\tau_w = \mu\, du/dy|_{y=0}$. From the previous definitions we found a frictional velocity of $u_\tau = 0.0125$ m/s. It is important to note that for this first attempt, only the heated single phase friction velocity was considered for all cases. Figure 9 shows the non-dimensional form utilizing the single phase heated frictional velocity ($u_\tau = 0.0125$ m/s). From this plot it is clear a significant difference from the single unheated case. These differences are attributed to the gravity driven flow induced in the vicinity of the heated wall. The effect of the boiling level in the liquid velocity was previously observed (Estrada-Perez & Hassan 2010). However, the present experiments focused in a single nucleation site, allowing to have different void fractions depending on the positions. Therefore, a single heat flux condition will provide different local void fractions, which simplified greatly the experimental and analysis work. In Figure 9 the red and gray lines represent the limits of the viscous sublayer and that of the buffer layer. Also, it is clear that the largest influence of the boiling bubbles is confined between the two lines. For the present conditions, it has been found that most of the boiling bubbles influence does not exceed the buffer layer. So it was decided to consider only those points below the edge of the buffer layer. As a first approach, multiple equations were fitted to these points with an automatic algorithm. Those equations with fewer numbers of coefficients and good fit were selected. This process will simplify the comparison of coefficients values with our measured bubbles parameters.

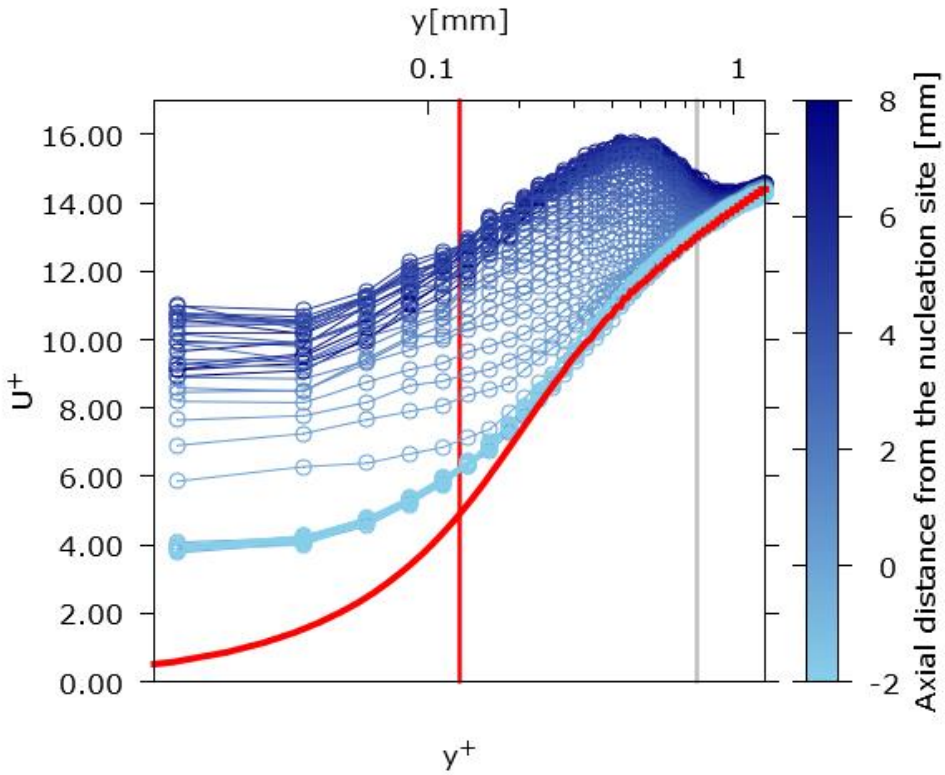


**Figure 9 semi-log plot of the axial liquid velocity profile at different axial positions from the nucleation site, and the single phase unheated law of the wall (red).**

## Conclusions

Using PTV, Shadowgraphy and Infrared Thermometry, the effect of different local void parameters on the liquid statistical quantities of subcooled boiling flow were studied.Velocity components, turbulence intensities, and Reynolds stresses are readily. The detailed information provided with the current experimental efforts is allowing the exploration of empirical correlations for the better description of the liquid behaviour under subcooled. . This work is an attempt to provide data of turbulent subcooled boiling flow for validation and improvement of two-phase flow computational models.

## *References*


Estrada-Perez, C. & Hassan, Y., 2010. PTV experiments of subcooled boiling flow through a vertical rectangular channel. *International Journal of Multiphase Flow*, 36, pp.691–706.

Koncar, B. & Krepper, E., 2008. CFD simulation of convective flow boiling of refrigerant in a vertical annulus. *Nuclear engineering and design*, 238, pp.693–706.

Koncar, B. & Tiselj, I., 2010. Influence of near-wall modelling on boiling flow simulation. *Nuclear Engineering and Design*, 240, pp.275–283.

Krogstadt, P.-Å. & Antonia, R., 1999. Surface roughness effects in turbulent boundary layers. *Experiments in Fluids*, 27, pp.450–460.

Marie, J., Moursali, E. & Tran-Cong, S., 1997. Similarity law and turbulence intensity profiles in a bubbly boundary layer at low void fractions. *International journal of multiphase flow*, 23, pp.227–247.

Mikielewicz, D., 2003. Hydrodynamics and heat transfer in bubbly flow in the turbulent boundary layer. *International journal of heat and mass transfer*, 46, pp.207–220.

Osterlund, J.M. et al., 2000. A note on the overlap region in turbulent boundary layers. *Physics of Fluids*, 12, p.1.

Sato, Y. & Sekoguchi, K., 1975. Liquid velocity distribution in two-phase bubble flow. *International Journal of Multiphase Flow*, 2, pp.79–95.

Dominguez-Ontiveros, E.E. et al., 2006. Development of a wall shear stress integral measurement and analysis system for two-phase flow boundary layers. Rev. of Scientific Inst., 77, p.105103.

Hassan, Y.A., Gutierrez-Torres, C.C. & Jimenez-Bernal, J.A., 2005. Temporal correlation modification by microbubbles injection in a channel flow. Int. Com. Heat Mass Transfer, 32, pp.1009–1015.

Končar, B., Kljenak, I. & Mavko, B., 2004. Modelling of local two-phase flow parameters in upward subcooled flow boiling at low pressure. Int. J. Heat Mass Transfer, 47, pp.1499–1513.

Koncar, B. & Krepper, E., 2008. CFD simulation of convective flow boiling of refrigerant in a vertical annulus. Nuclear engineering and design, 238, pp.693–706.

Koncar, B. & Matkovic, M., 2012. Simulation of turbulent boiling flow in a vertical rectangular channel with one heated wall. Nuclear Engineering and Design, 245, pp.131–139.

Koyasu, M. et al., 2009. Turbulence structure of bubbly upward flow (high spatial and temporal resolution measurements using high speed time series PTV). Transactions of the Japan Society of Mechanical Engineers, 75 part B, pp.1446–1453.

Lee, T.H., Park, G.C. & Lee, D.J., 2002. Local flow characteristics of subcooled boiling flow of water in a vertical concentric annulus. Int. J. Heat Mass Transfer, 28, pp.1351–1368.

Ortiz-Villafuerte, J. & Hassan, Y.A., 2006. Investigation of microbubble boundary layer using particle tracking velocimetry. J. Fluid Mechanics, 128, p.507.

Ramstorfer, F., Steiner, H. & Brenn, G., 2008. Modeling of the microconvective contribution to wall heat transfer in subcooled boiling flow. Int. J. Heat Mass Transfer, 51, pp.4069–4082.

Roy, R.P. et al., 2002. Turbulent subcooled boiling flow experiments and simulations. J. Heat Transfer, 124, p.73.

Roy, R.P., Hasan, A. & Kalra, S.P., 1993. Temperature and velocity fields in turbulent liquid flow adjacent to a bubbly boiling layer. Int. J. Multiphase Flow, 19, pp.765–795.

Roy, R.P., Velidandla, V. & Kalra, S.P., 1997. Velocity field in turbulent subcooled boiling flow. J. Heat Transfer, 119, p.754.

Wardana, I.N.G. et al., 1999. Turbulence structure in an annuli with strongly heated inner cylinder. Exp. Fluids, 27, pp.137–144.

Wardana, I.N.G., Ueda, T. & Mizomoto, M., 1994. Effect of strong wall heating on turbulence statistics of a channel flow. Exp. Fluids, 18, pp.87–94.

Wardana, I.N.G., Ueda, T. & Mizomoto, M., 1992. Structure of turbulent two-dimensional channel flow with strongly heated wall. Exp. Fluids, 13, pp.17–25.

Wardana, I.N.G., Ueda, T. & Mizomoto, M., 1995. Velocity-temperature correlation in strongly heated channel flow. Exp. Fluids, 18, pp.454–461.

Yeoh, G.H. et al., 2002. Prediction and measurement of local two-phase flow parameters in a boiling flow channel. Num. Heat Transfer, Part A, 42, pp.173–192.